

Analysis of Fluorescence Lifetime Imaging Microscopy (FLIM) Data Based on a Fully Automated Laguerre Deconvolution Method

P. Pande; C. A. Trivedi; J. A. Jo

Department of Biomedical Engineering, Texas A&M University, College Station, Texas, USA

Keywords

Fluorescence Lifetime Imaging Microscopy, Laguerre deconvolution, nonlinear least squares, optimization

Summary

Objectives: A novel Fluorescence Lifetime Imaging Microscopy (FLIM) deconvolution method based on the linear expansion of fluorescence decays on a set of orthonormal Laguerre functions was recently proposed. The Laguerre deconvolution method applies linear least-square estimation to estimate the expansion coefficients of all pixel decays simultaneously, performing at least two orders of magnitude faster than the other algorithms. In the original Laguerre FLIM deconvolution implementation, however, the Laguerre parameter α is selected using a heuristic ap-

proach, making it unsuitable for online applications.

Methods: In this study, we present a fully automated implementation of the Laguerre FLIM deconvolution, whereby the Laguerre parameter α is treated as a free parameter within a nonlinear least-squares optimization scheme.

Results: The performance of this method has been successfully validated on simulated data, and experimental FLIM images of standard fluorescent dyes and endogenous tissue fluorescence.

Conclusions: The main advantage of the proposed method is that it does not require any user intervention for tuning up the deconvolution process. Thus, we believe this method will facilitate the translation of FLIM to online applications, including real-time clinical diagnosis.

Correspondence to:

Javier A. Jo, Ph.D.
Department of Biomedical Engineering
Texas A&M University
3120 TAMU
College Station, Texas 77843
USA
E-mail: javierjo@tamu.edu

Methods Inf Med 2010; 49: 531–536

doi: 10.3414/ME09-02-0046

received: October 10, 2009

accepted: January 23, 2010

republished: July 20, 2010

1. Objectives

Fluorescence Lifetime Imaging Microscopy (FLIM) measures the time dynamics of the fluorescence emission across a sample area, allowing quantification of the spatial distribution of the sample fluorescence lifetime (lifetime maps). To estimate the lifetime maps, the FLIM data needs to be computationally processed by means of time deconvolution methods. A novel FLIM deconvolution method based on the linear expansion of the fluorescence decays on a set of orthonormal Laguerre functions was

recently proposed [1]. Accurate performance of this method depends on a proper selection of the set of orthonormal Laguerre functions, defined by the so-called Laguerre parameter, α . In the original Laguerre FLIM deconvolution implementation, however, α is selected using a heuristic approach, making it unsuitable for real-time applications. In a recent publication [3], a fully automated implementation of the Laguerre deconvolution for time-resolved fluorescence spectroscopy (TRFS) was presented. In this work, we extend the aforementioned research to FLIM,

whereby, in a similar way, the Laguerre parameter, α , is treated as a free parameter within a nonlinear least squares optimization scheme. The performance of this method has been validated on simulated data and experimental FLIM images of standard fluorescent dyes and endogenous tissue fluorescence.

2. Methods

2.1 Laguerre FLIM Deconvolution Method

In the context of time-domain FLIM, the series of time-gated fluorescence intensity maps $H(r, n)$ are given by the convolution of impulse response function (IRF) $h(r, n)$ with the instrument response $x(n)$:

$$H(r, n) = T \cdot \sum_{m=0}^{K-1} h(r, m) x(n-m) \quad (1)$$

where r denotes the pixel location, $n = 0, 1, \dots, N-1$ denotes the time gate, K determines the extent of system memory, T is the sampling interval and N is the number of time samples per pixel [1]. The Laguerre deconvolution technique uses a set of discrete Laguerre functions (DLFs) as the orthonormal basis to represent the IRF:

$$h(r, n) = \sum_{j=0}^{L-1} c_j(r) b_j^\alpha(n) \quad (2)$$

where $c_j(r)$ are the unknown Laguerre expansion coefficients (LEC) at pixel r , $b_j^\alpha(n)$ denotes the j -th order DLF [1] defined as shown in ► Figure 1 and L is the number of DLFs (order of Laguerre basis) used to model the IRF. The Laguerre parameter ($0 < \alpha < 1$) determines the rate of exponential decline of the DLFs and defines the time scale for which the Laguerre expansion of the system IRF is most efficient in terms of

Methods Inf Med 5/2010

$$b_j^\alpha(n) = \alpha^{(n-j)/2} (1-\alpha)^{1/2} \sum_{k=0}^j (-1)^k \binom{n}{k} \binom{j}{k} \alpha^{j-k} (1-\alpha)^k, \quad n \geq 0$$

Fig. 1 Equation 3

$$\mathbf{y}_r = \mathbf{V}_\alpha \mathbf{c}_r \tag{6}$$

Where,

$$\begin{bmatrix} y(r,0) \\ y(r,1) \\ \vdots \\ y(r,N-1) \end{bmatrix} = \begin{bmatrix} v_0^\alpha(0) & v_1^\alpha(0) & \dots & v_{L-1}^\alpha(0) \\ v_0^\alpha(1) & v_1^\alpha(1) & \dots & v_{L-1}^\alpha(1) \\ \vdots & \vdots & \ddots & \vdots \\ v_0^\alpha(N-1) & v_1^\alpha(N-1) & \dots & v_{L-1}^\alpha(N-1) \end{bmatrix} \begin{bmatrix} c_0(r) \\ c_1(r) \\ \vdots \\ c_{L-1}(r) \end{bmatrix} \tag{7}$$

$\mathbf{y}_r \qquad \mathbf{V}_\alpha \qquad \mathbf{c}_r$

Fig. 2 Equations 6 and 7

$$\mathbf{Y}_{modified} = \begin{bmatrix} y(0,1) & y(1,1) & \dots & y(N-1,1) \\ y(0,2) & y(1,2) & \dots & y(N-1,2) \\ \vdots & \vdots & \ddots & \vdots \\ y(0,M) & y(1,M) & \dots & y(N-1,M) \end{bmatrix}^T \tag{15}$$

$$\mathbf{E}_{modified} = \begin{bmatrix} \frac{d\boldsymbol{\varepsilon}_1}{d\alpha} & \frac{d\boldsymbol{\varepsilon}_2}{d\alpha} & \dots & \dots & \frac{d\boldsymbol{\varepsilon}_M}{d\alpha} \end{bmatrix}^T \tag{16}$$

Fig. 3 Equations 15 and 16

convergence [2]. For a given pixel r , the measured fluorescence decay $y(r, n)$ can thus be written as:

$$y(r, n) = H(r, n) = \sum_{j=0}^{L-1} c_j(r) v_j^\alpha(n) \tag{4}$$

where

$$v_j^\alpha(n) = T \cdot \sum_{m=0}^{K-1} b_j^\alpha(m) x(n-m). \tag{5}$$

Then, the system of linear equations defined in Equation 4 can be expressed in a matrix notation as can be seen in ►Figure 2.

To include the effect of experimental noise we modify Equation 6 as:

$$\mathbf{y}_r = \mathbf{V}_\alpha \mathbf{c}_r + \boldsymbol{\varepsilon}_r \tag{8}$$

where $\boldsymbol{\varepsilon}_r$ is the error vector resulting due to noise at the r -th pixel.

We are interested in obtaining the IRF, or equivalently the LEC vector, \mathbf{c}_r . The correct estimation of LEC depends on proper selection of the set of DLFs, which in turn depends on proper choice of Laguerre parameter, α .

2.2 Defining and Optimizing the Cost Function

Equation 8 can be solved to get the least squares estimate of the measured decay \mathbf{y}_r , which is equal to:

$$\hat{\mathbf{y}}_r = \mathbf{V}_\alpha (\mathbf{V}_\alpha^T \mathbf{V}_\alpha)^{-1} \mathbf{V}_\alpha^T \mathbf{y}_r \tag{9}$$

The cost function at the r -th pixel is then defined as the mean square error of the estimated decay:

$$F^r(\alpha) = (\mathbf{y}_r - \hat{\mathbf{y}}_r)^T (\mathbf{y}_r - \hat{\mathbf{y}}_r) = \mathbf{y}_r^T \boldsymbol{\varepsilon}_r \tag{10}$$

It must be reiterated that all the analysis until now focuses on one pixel of the FLIM image. If we denote the number of pixels by M then the cost function for the FLIM image can be written as a sum of cost functions of individual pixels:

$$F_{image}(\alpha) = F^1(\alpha) + F^2(\alpha) + \dots + F^M(\alpha) \tag{11}$$

Our objective is to find the value of α that minimizes the cost function defined in Equation 11. We denote this optimum value of α by $\hat{\alpha}$. Mathematically, this problem can be stated as:

$$\hat{\alpha} = \arg \min_{\alpha} F_{image}(\alpha) \tag{12}$$

The problem stated in Equation 12 can be framed as a nonlinear least-squares optimization problem. Since α is constrained in $(0, 1)$, we implemented a simple iterative gradient-based optimization scheme, where the search direction and step size is determined using successive bisection algorithm. This iterative process can be summarized as:

$$\hat{\alpha}^{(v+1)} = \hat{\alpha}^{(v)} - \gamma^{(v)} \left[\frac{d}{d\alpha} (F_{image}(\alpha)) \right]^{(v)} \tag{13}$$

where, $\hat{\alpha}^{(v)}$ and $\gamma^{(v)}$ denote the estimated value of α and the step size at v -th iteration. Next, we find an expression for the derivative of the cost function. Here, we briefly outline the method of obtaining such an expression. For a more detailed derivation, interested readers are referred to our recent publication [3] wherein a different but similar expression is derived for time-resolved fluorescence spectroscopy measurements.

It follows from Equations 10 and 11 that:

$$\frac{d}{d\alpha} (F_{image}(\alpha)) = \sum_{r=1}^M \mathbf{y}_r^T \left(\frac{d\boldsymbol{\varepsilon}_r}{d\alpha} \right) \tag{14}$$

If we then define two matrices $\mathbf{Y}_{modified}$ and $\mathbf{E}_{modified}$ as shown in ►Figure 3, it can be shown that each term of the summation in Equation 14 corresponds to a diagonal

term of the matrix product $\mathbf{Y}_{modified}^T \mathbf{E}_{modified}$. It then follows that the summation in the RHS of Equation 14 can be written as:

$$\frac{d}{d\alpha}(F_{image}(\alpha)) = trace(\mathbf{Y}_{modified}^T \mathbf{E}_{modified}) \quad (17)$$

To evaluate $\mathbf{E}_{modified}$ we define another matrix $\mathbf{C}_{modified}$ as:

$$\mathbf{C}_{modified} = \begin{bmatrix} c_0(1) & c_0(2) & \dots & c_0(M) \\ c_1(1) & c_1(2) & \dots & c_1(M) \\ \vdots & \vdots & \ddots & \vdots \\ c_{L-1}(1) & c_{L-1}(2) & \dots & c_{L-1}(M) \end{bmatrix} \quad (18)$$

Following the derivation in [3], we can write an expression for $\mathbf{E}_{modified}$ as can be seen in ►Figure 4.

Finally, to evaluate $\frac{d\mathbf{V}_a}{d\alpha}$ and $\frac{d\mathbf{V}_a^T}{d\alpha}$ we use the recursive property of the DLF [2] as shown in ►Figure 5.

Using Equations 17–21 in Equation 13, we can estimate the optimal value of α .

For the analyses presented in the next section, we fixed the order of Laguerre expansion basis to 4, based on findings from previous studies [3].

2.3 Instrumentation for FLIM Measurements

FLIM imaging was accomplished using a time-domain wide-field time-gated endoscopic FLIM instrument [5]. The central

component of the FLIM system was an intensified CCD camera (4Picos, Stanford Computer Optics) coupled to a flexible endoscope through a microscope objective (20×). The endoscope was constructed from a 10,000-fiber coherent bundle (O.D. 400 μm) glued to a GRIN lens (NA 0.5, 4 mm working distance). Light pulse excitation was delivered via a multimode fiber (NA 0.22, O.D. 200 μm). A filter wheel inserted in the collimated optical path was used for multispectral imaging at the pre-defined emission bands of 390, 450 and 550 nm. A N2 UV laser (337 nm, 0.8 ns FWHM, 50 Hz rep rate, 5 μJ/pulse) was used for excitation. The FLIM images were acquired with a time resolution of 200 ps. For imaging the dyes, the dye solution was placed in a quartz cuvette illuminated from one side, while the endoscope was positioned on the other side of the cuvette. For tissue imaging, coronary segments from a human heart were harvested from autopsy cases. The coronary artery was opened longitudinally for luminal imaging. The coronary plaques were imaged by placing the endoscope tip perpendicular to the lumen side, resulting in a circular field of view of ~2 mm. For each sample, FLIM images corresponding to the peak emission band of that fluorophore were recorded. The laser pulse energy at the tip of the excitation fiber probe was adjusted to ~5 μJ/pulse.

3. Results

3.1 Testing on Synthetic FLIM Images

A synthetic FLIM image of 25 × 25 pixels was generated using a bi-exponential model (lifetimes 1 ns and 4 ns) with relative contributions varying in a linear fashion (from 1 ns at the lower leftmost to 4 ns at the top leftmost pixel). Gaussian noise of zero mean was added to yield two images at 40 dB and 25 dB SNR. A representative Gaussian instrument response was used to form the synthetic FLIM images.

►Figure 6a shows the theoretically calculated lifetime map. For a mixture of two fluorophores of relative contribution β , ($0 \leq \beta \leq 1$) and $(1 - \beta)$, and lifetime τ_1 and τ_2 respectively; the lifetime of the mixture is given by [4]:

$$\tau_{mixture} = \frac{\beta\tau_1^2 + (1 - \beta)\tau_2^2}{\beta\tau_1 + (1 - \beta)\tau_2} \quad (22)$$

The synthetic data was then deconvolved using the proposed deconvolution algorithm to estimate the IRF and thereafter the lifetime map was calculated from the estimated IRFs. Optimal value of α was found to be 0.825 and 0.834 for 40 dB and 25 dB noise levels respectively. ►Figure 6d shows the measured decay at a sample pixel, the instrument response profile, and the estimated decay. The inset also shows the estimated IRF, the residuals and the autocorre-

Fig. 4 Equation 19

$$\mathbf{E}_{modified} = \frac{d\mathbf{V}_a}{d\alpha} \mathbf{C}_{modified} + \mathbf{V}_a (\mathbf{V}_a^T \mathbf{V}_a)^{-1} \left[\frac{d\mathbf{V}_a^T}{d\alpha} \mathbf{Y}_{modified} - \left(\frac{d\mathbf{V}_a^T}{d\alpha} \mathbf{V}_a + \mathbf{V}_a^T \frac{d\mathbf{V}_a}{d\alpha} \right) \mathbf{C}_{modified} \right]$$

Fig. 5 Equations 20 and 21

$$\frac{dv_j^\alpha(n)}{d\alpha} = \frac{1}{2\sqrt{\alpha}} (v_j^\alpha(n-1) + v_{j-1}^\alpha(n)) + \sqrt{\alpha} \left(\frac{dv_j^\alpha(n-1)}{d\alpha} + \frac{dv_{j-1}^\alpha(n)}{d\alpha} \right) - \frac{dv_{j-1}^\alpha(n)}{d\alpha} \quad (20)$$

When,

$$\frac{dv_0^\alpha(n)}{d\alpha} = \frac{1}{2\sqrt{\alpha}} (v_0^\alpha(n-1)) + \sqrt{\alpha} \left(\frac{dv_0^\alpha(n-1)}{d\alpha} \right) + \frac{1}{2\sqrt{1-\alpha}} x(n) \quad (21)$$

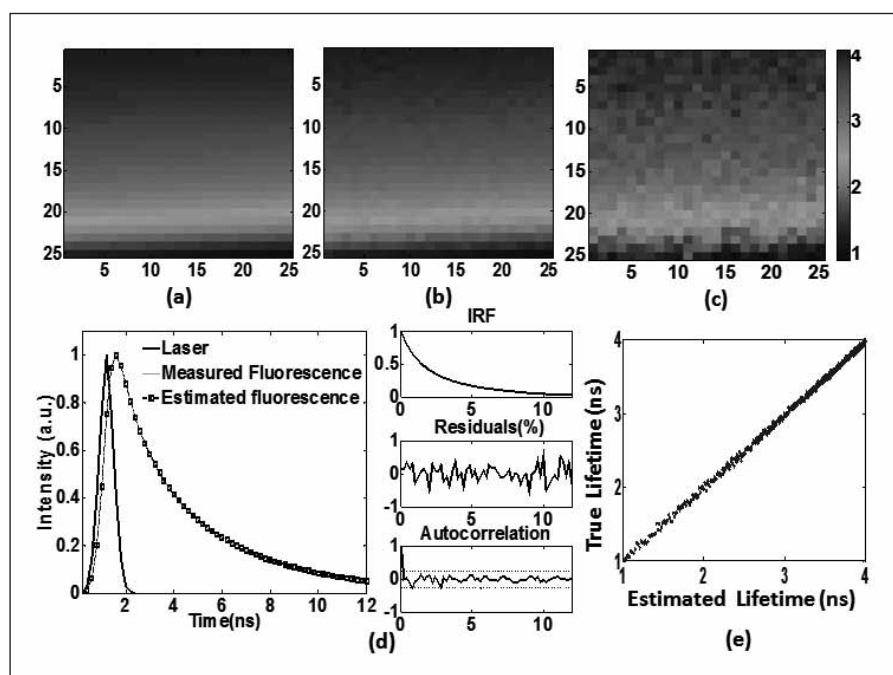


Fig. 6 a) Theoretically calculated lifetime map. b) Estimated lifetime map at 40 dB SNR. c) Estimated lifetime map at 25 dB SNR. d) Measured decay at a sample pixel and the estimated fit. Also shown is the laser pulse, estimated IRF and the error residuals. e) Correlation between the true and estimated lifetime values at 40 dB SNR.

lation for the estimation. The normalized residuals ($<1\%$) and their autocorrelation functions showed a significant random behavior, indicating good fitting attained by our method. ▶ Figures 6b and 6c show the lifetime maps at 40 dB and 25 dB SNR noise levels calculated from the estimated IRFs at the corresponding noise levels, respectively. Both calculated lifetime maps resembled the true lifetime maps, showing values from ~ 4 ns at the top left corner to ~ 1 ns at the bottom right corner, as expected; however, the lifetime map was less accurate for the low SNR condition. ▶ Figure 6e shows the corresponding correlation plots for the true (theoretical) and calculated lifetimes for 40 dB SNR indicating good agreement between the calculated and true lifetime values.

3.2 FLIM Images of Fluorescence Standards

Results of the analysis of FLIM images from the solution of flavin adenine dinucleotide (FAD) in phosphate-buffered saline (PBS) and 9-cyanoanthracene (9-CA) in ethanol are presented in ▶ Figure 7 (top and bottom panels, respectively). Histograms of the lifetime maps (center panels) for both FAD and 9-CA are shown in the rightmost panels. The histograms were centered at 2.61 ns and 11.92 ns for FAD and 9-CA, respectively. These average lifetime values are in good agreement with those obtained from spectroscopy measurements of equivalent solutions with a time-resolved fluorescence spectroscopy (TRFS) system as previously reported [5]. We also tested our algorithm on FLIM data obtained from solutions of NADH in PBS and Rhodamin B (RhB) in ethanol (listed in ▶ Table 1).

The results of the present study have been summarized and compared with those reported in an earlier study [5] in ▶ Table 1. The computational time in case of 9-cyanoanthracene (9-CA) is much more than other fluorophores because the large lifetime (~ 11 ns) of 9-CA demands an acquisition and processing of a larger number of FLIM images as compared to fluorophores with relatively shorter lifetimes. To further reduce the computational time, we also tried to perform the optimi-

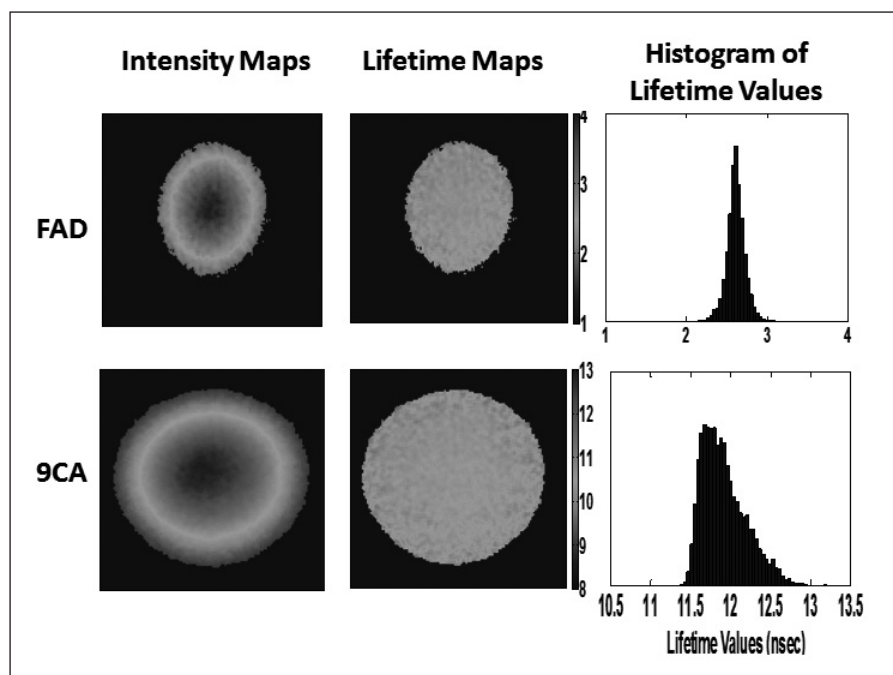


Fig. 7 Analysis of FLIM images from FAD in PBS and 9CA in ethanol. Leftmost panels show the intensity maps for FAD (upper leftmost) and 9CA (lower leftmost); middle panels their corresponding lifetime maps (values in nsec), and the rightmost panels are the histograms of the lifetime values indicating the distribution of lifetimes.

zation on compressed FLIM images (compressed three times, by averaging pixel values in a 3×3 region). In such a case, it was found that such compression did not affect the estimation of the optimal values for α , while significantly reducing the computational time (37.6 s for 9-CA and ~ 1.5 s to 8.5 s for the rest).

3.3 FLIM Images from Human Artery

Analysis of the FLIM images from a post-mortem human artery is presented in Figure 8. The image indicated two biochemically distinct areas with variation in both the normalized fluorescence intensity and lifetimes. One area (ROI-1) was characterized by high normalized emission intensity at 400 nm and weaker emission at 450 nm and 500 nm; long lifetimes (~ 3.0 ns) at 400 nm and short lifetimes at 450 nm and 500 nm (~ 2.0 ns). The other area (ROI-2) was characterized by similar normalized emission intensity at 400 nm and 450 nm and weaker emission at 500 nm; short lifetimes in all bands (~ 2.0 ns for 400 nm, ~ 1.4 ns for 450 nm and ~ 1.6 ns for 500 nm). The fluorescence characteristics of ROI-1 resembled the fluorescence emission of collagen, showing a narrow peak emission and long lifetime at ~ 400 nm, and shorter lifetime at longer emission wavelengths whereas the fluorescence characteristics of ROI-2 resembled the fluorescence emission of collagen and elastin [6, 7]. These observations were in good agreement with the histopathology finding: the middle area (ROI-1) correlated with the collagen-rich thick fibrotic plaque section, while the bottom area (ROI-2) correlated with the thinner section of the plaque, where the fluorescence is originated from both the intima's collagen and the media's elastin.

4. Conclusion

In this paper, we introduce a fully automated deconvolution method for FLIM data analysis based on an iterative implementation of the Laguerre deconvolution technique. In this new implementation, the

Table 1 Fluorescence lifetime values of standard dyes

Sample	Peak (nm)	Optimal α	$\tau_{\text{calculated}}$ (ns)	$\tau_{\text{literature}}$ (ns)	Computation time (s)
9-CA	450 ± 20	0.953	11.92 ± 0.28	11.70 – 11.80	211.6
RhB	550 ± 20	0.732	2.49 ± 0.08	2.60 – 3.01	44.4
FAD	450 ± 20	0.788	2.61 ± 0.11	2.30 – 2.85	48.6
NADH	400 ± 20	0.273	0.41 ± 0.01	0.30 – 0.40	7.1

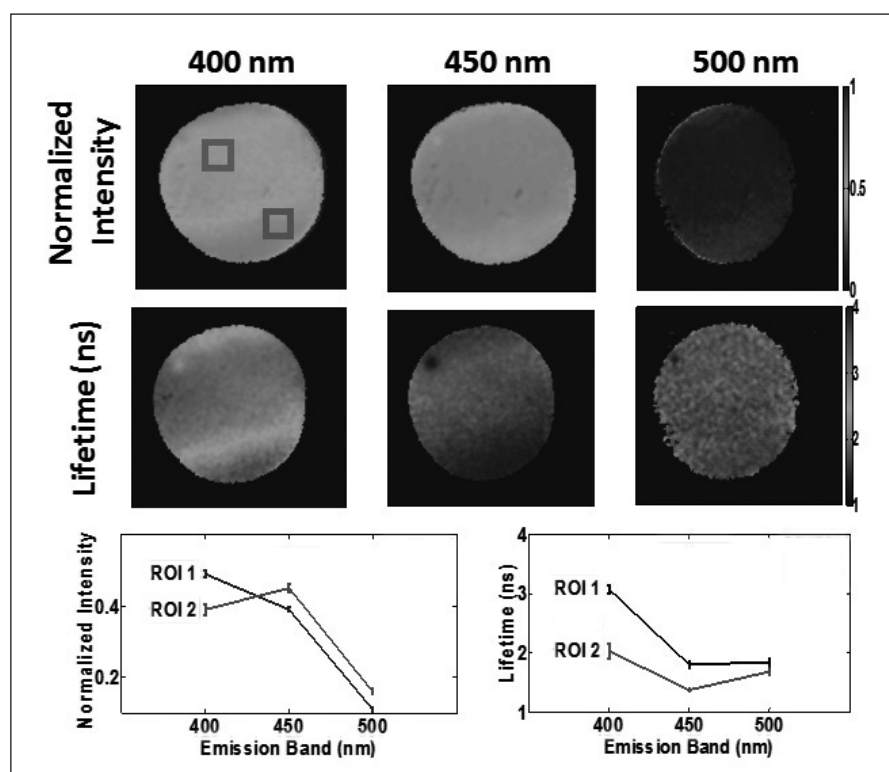


Fig. 8 Analysis of FLIM images of a fibrotic plaque in human artery. The FLIM maps show a middle section of the plaque rich in collagen (ROI-1), and a bottom section rich in both elastin and collagen (ROI-2) corresponding to the thinner side of plaque.

optimization of the Laguerre parameter is performed as part of the deconvolution routine. The proposed automated Laguerre deconvolution method performs a non-linear least-square search for the optimal values of α to guarantee that the fluorescence IRF is properly expanded and estimated. Our validation results on FLIM data from fluorescence lifetime standards and tissue endogenous fluorophores showed that our proposed algorithm is capable of converging first to an optimal value of using non-linear least square optimization, and then to an optimal fluorescence IRF expansion using linear least-square esti-

mation of the expansion coefficients. This is an important improvement over previous implementation of the Laguerre deconvolution method, in which the value of α is determined by trial and error. The optimization of α ensures an accurate and automated estimation of the fluorescence IRF.

To summarize, we have presented a fully automated deconvolution method for FLIM. The method has been validated on FLIM data from fluorescence lifetime standards, tissue endogenous fluorophores and a biological tissue sample. The main advantage of the proposed method is that it

does not require any user intervention for tuning up the deconvolution process. The proposed method thus offers an opportunity to realize online analysis of FLIM data and will facilitate the use of Fluorescence Lifetime Imaging Microscopy in real-time applications. Current efforts in our research group focus on the applications of this method to facilitate the use of FLIM for clinical diagnosis of cardiovascular diseases and epithelial cancer.

Acknowledgments

This work was supported by the American Heart Association – Texas Affiliate, Beginning Grant-in-Aid Grant 0765102Y and the NIH Grant 1-R21-CA132433.

References

1. Ramanujan VK, Jo JA, Cantu G, Herman BA. Spatially resolved fluorescence lifetime mapping of enzyme kinetics in living cells. *J Microsc* 2008; 230 (Pt 3): 329–338.
2. Marmarelis VZ. Identification of nonlinear biological systems using Laguerre expansions of kernels. *Ann Biomed Eng* 1993; 21 (6): 573–589.
3. Dabir AS, Trivedi CA, Ryu Y, Pande P, Jo JA. Fully automated deconvolution method for on-line analysis of time-resolved fluorescence spectroscopy data based on an iterative Laguerre expansion technique. *J Biomed Opt* 2009; 14 (2): 024030.
4. Lakowicz J. *Principles of Fluorescence Spectroscopy*. Springer; 2006.
5. Fang QY, Papaioannou T, Jo JA, Vaitha R, Shastry K, Marcu L. Time-domain laser-induced fluorescence spectroscopy apparatus for clinical diagnostics. *Review of Scientific Instruments* 2004; 75 (1): 151–162.
6. Arakawa K, Isoda K, Ito T, Nakajima K, Shibuya T, Ohsuzu F. Fluorescence analysis of biochemical constituents identifies atherosclerotic plaque with a thin fibrous cap. *Arterioscler Thromb Vasc Biol* 2002; 22 (6): 1002–1007.
7. Marcu L, Jo JA, Fang Q, Papaioannou T, Reil T, Qiao JH, et al. Detection of rupture-prone atherosclerotic plaques by time-resolved laser-induced fluorescence spectroscopy. *Atherosclerosis* 2009; 204 (1): 156–164.